ARTICLE

# Theoretical study of the mechanism of the solvent dependency of ESIPT in HBT†

Received 00th January 20xx,
Accepted 00th January 20xx

DOI: 10.1039/x0xx00000x

Keiji Naka,[a] Hirofumi Sato,[a,b,c] and Masahiro Higashi *[a,b]

2-(2′-hydroxyphenyl)-benzothiazole (HBT) has been widely studied for use as a system for excited-state intramolecular proton transfer. However, the mechanism underlying the solvent dependency of HBT fluorescence spectra remains unclear. In this study, the HBT photochemical process in the $S_1$ state was analysed using density functional theory (DFT) and time-dependent density functional theory (TDDFT). The excited-state intramolecular proton transfer in the enol form of HBT was found to depend on the hydrogen-bond acceptability of the solvent. The twisting of the keto form of HBT is determined by whether HBT acts as a hydrogen-bond acceptor or donor. A specific stacking structure of the enol form of HBT was found to decrease the $S_1 \rightarrow S_0$ transition energy, which corresponds to the experimental fluorescence spectra in a DMSO/$H_2O$ solution mixture.

## Introduction

Excited-state intramolecular proton transfer (ESIPT) molecules have been widely studied because of various applications, such as luminescence materials[1–5] and molecular probes[6,7]. 2-(2′-hydroxyphenyl)-benzothiazole (HBT) is a typical ESIPT molecule that has been intensively studied in various fields[8–21]. Figure 1 shows the ESIPT process in HBT. HBT exists in the enol form at the $S_0$ ground state. After HBT absorbs light and is excited to the $S_1$ state, the enol form of HBT is converted into the keto form, and the proton bonded to the oxygen atom in the enol form is transferred to the nitrogen atom. After the keto HBT emits energy and relaxes to the $S_0$ state, HBT returns to the enol form.

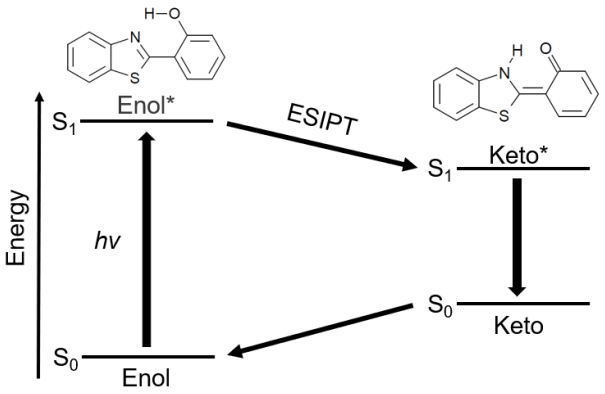


Figure 1. ESIPT process in HBT.

This intramolecular proton transfer process is known to be a four-level cyclic proton-transfer process (E-E*-K*-K- E)[22,23].

Keto HBT can relax from the $S_1$ to the $S_0$ state in two ways: internal conversion and fluorescence. Barbatti et al. experimentally investigated the HBT relaxation process[3] and observed time-resolved transmission changes of keto HBT in the gas phase and in cyclohexane at 560 nm after excitation at 325 nm. Keto HBT relaxes from the $S_1$ to the $S_0$ state within 5 ps in the gas phase, compared to approximately 100 ps in cyclohexane. This experimental result shows that internal conversion in HBT dominates in the gas phase but is not favourable in solution.

The internal conversion process of HBT in the gas phase has been well studied theoretically[4,14–19]. First, ESIPT proceeds after the excitation to the $S_1$ state. Next, the central C=C bond of HBT twists, such that the energy gap between $S_1$ and $S_0$ states decreases and is close to zero around a conical intersection. HBT then relaxes to the $S_0$ state through the conical intersection. The

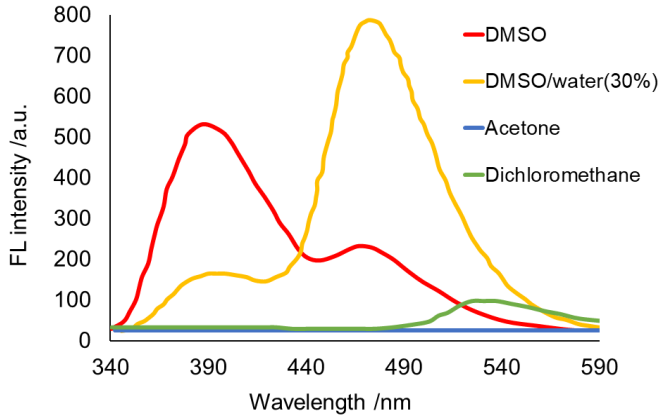


Figure 2. The experimental fluorescence spectrum of HBT in solutions. The data were traced from Ref 8.

[a] Department of Molecular Engineering, Graduate School of Engineering, Kyoto University, Kyoto 615-8510, Japan. E-mail: higashi@moleng.kyoto-u.ac.jp
[b] Elements Strategy Initiative for Catalysts and Batteries (ESICB), Kyoto University, Kyoto 615-8520, Japan.
[c] Fukui Institute for Fundamental Chemistry, Kyoto University, Kyoto 606-8103, Japan.

† Electronic supplementary information (ESI) available: See DOI:

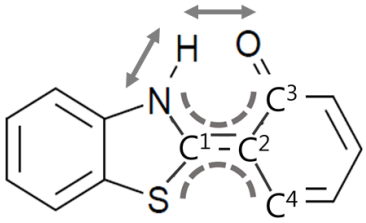


$$R_{pt} = R_{OH} - R_{NH}$$

$$\theta = \frac{D(N,C^1,C^2,C^3) + D(S,C^1,C^2,C^4)}{2}$$

Figure 3. The definitions of reaction coordinates of proton transfer and C=C twisting.

C=C twisting process is related to internal conversion and is often found in other molecules, such as stilbene[24–26] and retinal[27–29].

However, the relaxation process of HBT in solution remains unclear[8,9]. HBT fluorescence spectra have been experimentally shown to be strongly solvent-dependent[8] (Figure 2). For example, the enol spectrum is dominant in DMSO solution, whereas the keto spectrum is obtained in $CH_2Cl_2$ solution. No spectral peaks are observed in acetone solution. Among these three solvents, DMSO is the most polar, followed by acetone and then $CH_2Cl_2$. Therefore, it is difficult to explain the absence of fluorescence in $CH_2Cl_2$ only in terms of solvent polarity.

The addition of water to a DMSO solution of HBT is known to induce HBT aggregation[8]. As more HBT aggregates, the most intense peak corresponding to the enol form decreases, and the second-most intense peak with a longer wavelength becomes more dominant (Figure 2). The wavelength of the second-most intense peak is much shorter than that of the keto peak in other solutions[5]; thus, the origin of this peak is unclear.

The purpose of this study is to elucidate the molecular mechanism of the solvent dependency of HBT fluorescence spectra with theoretical methods. The solvent dependency of HBT has not been theoretically investigated thus far, to the best of our knowledge. Three solvents, DMSO, acetone and $CH_2Cl_2$ were considered in the calculations. First, we calculated the energy profiles of ESIPT along the reaction coordinates by using time-dependent density functional theory (TDDFT) and the polarizable continuum model (PCM)[30–32]. As C=C twisting in HBT induces internal conversion, we considered not only the ESIPT but also C=C twisting motion. Second, we investigated the intermolecular hydrogen bonds and interaction energies between HBT and a solvent molecule. We analysed the energy

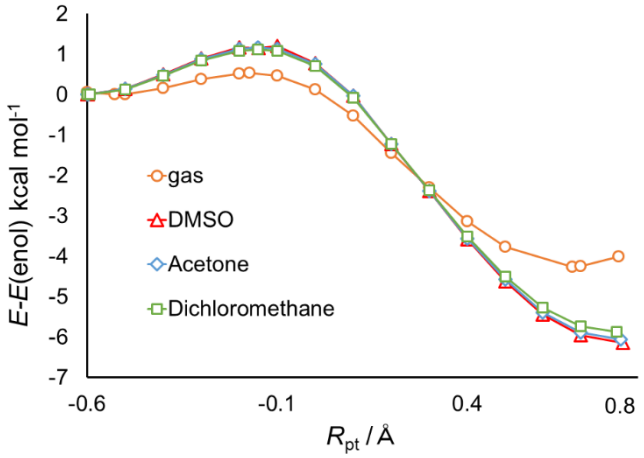


Figure 4. Calculated energy profiles along ESIPT in the gas phase and in solutions at the ωB97X-D/6-31G(d,p) level.

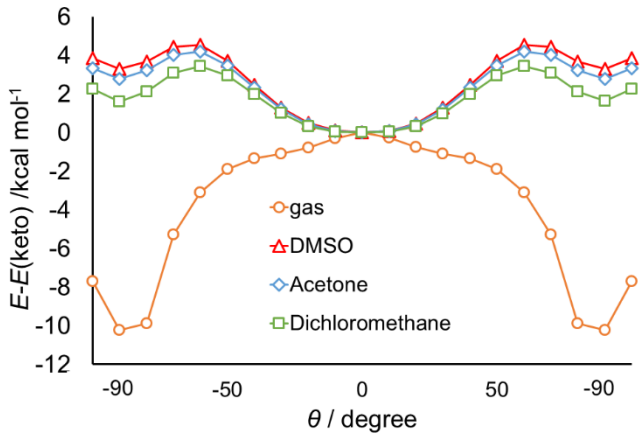


Figure 5. Calculated $S_1$ energy profiles along C=C twisting at the ωB97X-D/6-31G(d,p) level.

gaps of two stacked HBT aggregates to investigate how HBT aggregation affects the fluorescence spectra.

## Method

DFT and TDDFT were used to determine the ground and excited states of HBT. We mainly adopted the ωB97X-D functional[33] to include long-range correction and dispersion effects. Both these effects are important to accurately describe the excited states of HBT-solvent complexes and HBT aggregates, which cannot be reproduced with the conventional B3LYP and CAM-B3LYP functionals. For comparison, we also used the M11 range-separated functional[34] and EOM-CCSD method[35]. The 6-31G(d,p) basis set was mainly used, and the 6-311G(d,p) basis set was used to calculate the intermolecular interaction

Table 1. Calculated activation energies of ESIPT $\Delta E_{pt}$ and C=C twisting $\Delta E_{tw}$ at the ωB97X-D/6-31G(d,p) level (in kcal/mol).

| Solvent | gas | DMSO | Acetone | $CH_2Cl_2$ |
|---|---|---|---|---|
| $\Delta E_{pt}$ | 0.53 | 1.16 | 1.18 | 1.13 |
| $\Delta E_{tw}$ | No barrier | 4.56 | 4.21 | 3.45 |

Table 2. Calculated energy differences between $HBT_{out}$ and the enol form, $E_{out}$-$E_{enol}$ (in kcal/mol) at the ωB97X-D/6-31G(d,p) level.

| Solvent | DMSO | Acetone | $CH_2Cl_2$ |
|---|---|---|---|
| $E_{out}$-$E_{enol}$ | 12.32 | 12.58 | 13.15 |

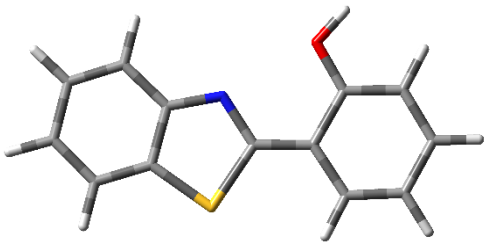

Figure 6. $HBT_{out}$ structure.

energies between HBT and a solvent molecule. The solvent effect was incorporated by using the integral equation formalism model of PCM (IEFPCM). We defined the reaction coordinate for proton transfer, $R_{pt}$, as the difference between OH and NH bonds (Figure 3) and calculated the energy profiles for ESIPT in HBT along $R_{pt}$. The enol and keto forms correspond to negative and positive $R_{pt}$, respectively. We defined a reaction coordinate θ as the average between the two dihedral angles $D(N,C^1,C^2,C^3)$ and $D(S,C^1,C^2,C^4)$ to investigate C=C twisting in keto HBT. We calculated the intermolecular interaction energy between HBT and a solvent molecule, considering both the enol and keto forms of HBT (see below). We investigated the $S_1 \rightarrow S_0$ energy gap of two stacked HBT aggregates for four conformations. All the quantum calculations were carried out using the Gaussian 16 program package.[36]

## Results and discussion

### Energy surfaces of intramolecular proton transfer and C=C twisting

Figure 4 shows the calculated energy profiles for ESIPT in the gas phase and solutions at the ωB97X-D/6-31G(d,p) level. Here all other geometries except $R_{pt}$ are optimized in the $S_1$ state. The transition states are located at $R_{pt}$ = −0.171, −0.149, −0.151, and −0.151 Å in the gas phase, DMSO, acetone, and $CH_2Cl_2$, respectively. The activation energies from the enol to keto forms, $\Delta E_{pt}$, are shown in Table 1. The activation energies in the three solutions are quite similar, at ~1.1 kcal/mol, which is slightly larger (~0.5 kcal/mol) than that in the gas phase. The remarkable solvent dependency did not appear in these calculation results.

Figures 5 and S1 (in ESI†) show the $S_1$ and $S_0$ energy profiles for C=C twisting of the keto form optimized in the $S_1$ state at the ωB97X-D/6-31G(d,p) level. Along $S_1$ state C=C twisting, no activation barrier is found at $-90° \le \theta \le 90°$ in the gas phase. That is, the keto form of HBT is smoothly twisted, and the energy gap between $S_1$ and $S_0$ decreases in the gas phase, which is consistent with the results of previous studies[14,16–19]. By contrast, activation barriers are found for HBT in the three solutions. The activation energies are 4.56, 4.21 and 3.45 kcal/mol in DMSO, acetone and $CH_2Cl_2$, respectively (Table 1). The planar keto form is more stable than the twisted form in solution. However, the striking solvent dependency also did not manifest in these calculation results, as for the ESIPT results.

The intramolecular proton transfer and C=C twisting energy profiles calculated with M11 functional and EOM-CCSD method were found to be similar to those with ωB97X-D functional (Figs S2-S7 and Tables S1 and S2). In addition, the energy profiles in the gas phase are similar to those in the previous studies[14,16–19]. Therefore, the dependence on the calculation method is considered to be small.

### Inadequacy of PCM for intramolecular hydrogen bonds

We analysed the energy profiles for intramolecular proton transfer and C=C twisting in the $S_1$ state. However, the experimentally observed solvent dependency was still not observed. We considered the possibility that an intermolecular hydrogen bond between HBT and a solvent molecule disturbs ESIPT, because DMSO and acetone can act as hydrogen-bond acceptors as suggested in the previous study[37]. Therefore, we investigated the stability of $HBT_{out}$, a conformer with an outwardly directed OH bond (Figure 6), in solution, where the intermolecular hydrogen bond was implicitly considered using PCM. Table 2 shows the energy differences between $HBT_{out}$ and the normal enol form in the three solutions. The energy differences are 12-13 kcal/mol in all cases, indicating that $HBT_{out}$ was considerably more unstable than the enol form. Considering the difference between intra- and intermolecular hydrogen bonds, $HBT_{out}$ should be more stable in DMSO and acetone solutions. These calculated results demonstrate the inadequacy of PCM in these cases. PCM cannot be used to describe strong intermolecular interactions, such as hydrogen bonds, because the solvent is treated as a uniformly distributed dielectric. This inadequacy are often been identified in previous studies[38–40]. Therefore, we explicitly treated the solvent molecules and determined the contributions of the intermolecular hydrogen bond between HBT and a solvent molecule, as discussed below.

### Intermolecular interaction energies between HBT and solvents

First, we discuss the interaction energies between the enol form of HBT and solvent molecules, which are summarized in Table 3. The interaction energy in the $S_1$ state was defined as the difference between the $S_1$ energy of complex and the sum of $S_1$ energy of HBT and $S_0$ energy of solvent. Note that the enol HBT corresponds to the $HBT_{out}$ in the above section. It is also noted that we treated one solvent molecule explicitly because the OH group of enol HBT can make a hydrogen bond with only one solvent molecule (see also below). Several methods were employed, and the results were compared to ensure reliability.

Table 3. Calculated interaction energies between the enol HBT and solvent molecules (in kcal/mol).

| | DMSO | | Acetone | | $CH_2Cl_2$ | |
|---|---|---|---|---|---|---|
| Calculation level | $S_0$ | $S_1$ | $S_0$ | $S_1$ | $S_0$ | $S_1$ |
| ωB97X-D/6-31G(d,p) | −5.61 | −2.95 | −4.04 | 0.08 | 2.37 | 7.23 |
| ωB97X-D/6-311G(d,p) | −10.63 | −3.86 | −4.22 | −0.08 | 1.84 | 6.21 |
| PCM-ωB97X-D/6-31G(d,p) | −3.63 | −1.63 | −3.81 | −1.30 | 1.38 | 4.02 |
| PCM-ωB97X-D/6-311G(d,p) | −4.23 | −2.05 | −3.85 | −1.36 | 0.12 | 2.66 |

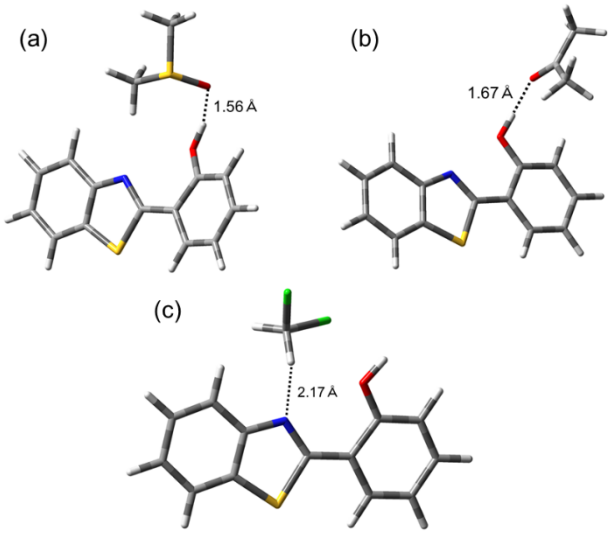


Figure 7. Optimized geometries of the complexes between enol HBT and (a) DMSO, (b) acetone, or (c) $CH_2Cl_2$ at the ωB97X-D/6-31G(d,p) level. Distances are in Å.

The interaction energies between enol HBT and DMSO in the $S_0$ state obtained by all the methods are significantly negative, below −3 kcal/mol, indicating that enol HBT strongly interacts with DMSO in the $S_0$ state. The interaction energies in the $S_1$ state are slightly weaker, but still negative, irrespective of the calculation method used. This result shows that the HBT forms a stable intermolecular hydrogen bond with a DMSO molecule (Figure 7) in both the $S_0$ and $S_1$ states. Therefore, ESIPT of the intermolecular hydrogen bond between HBT and DMSO is prevented, which is consistent with the experimental result. By contrast, all the calculated interaction energies between HBT and $CH_2Cl_2$ are positive for both the $S_0$ and $S_1$ states. These results demonstrate that enol HBT does not interact with a $CH_2Cl_2$ molecule by forming a hydrogen bond, such that the ESIPT is not disturbed in $CH_2Cl_2$ solution. The negative interaction energies between HBT and acetone in the $S_0$ state indicate that enol HBT forms an intermolecular hydrogen bond with an acetone molecule. However, the calculated interaction energies are close to zero in the $S_1$ state: the values obtained for ωB97X-D/6-31G(d,p), ωB97X-D/6-311G(d,p), PCM-ωB97X-D/6-31G(d,p) and PCM- ωB97X-D/6-311G(d,p) are 0.08, −0.08, −1.30, and −1.36 kcal/mol, respectively. Therefore, even if there is an interaction between HBT and acetone, it can be considered to be very weak, and ESIPT can proceed. This interaction strength is consistent with the hydrogen-bond acceptability of the solvent. Namely, ESIPT is prevented by DMSO, which has a high hydrogen-bond acceptability, but not by $CH_2Cl_2$ and acetone, which have lower hydrogen-bond acceptabilities.

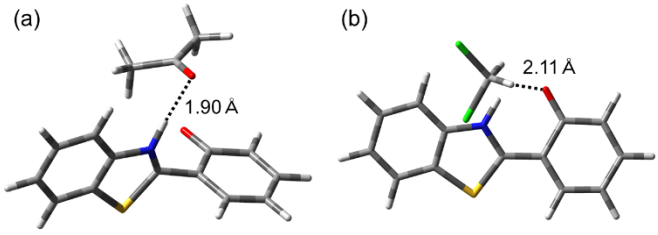


Figure 8. Optimized geometries of complexes between the keto HBT and (a) acetone or (b) $CH_2Cl_2$ at the ωB97X-D/6-31G(d,p) level. Distances are in Å.

Table 4. Calculated interaction energies $E_{int}$ between the keto HBT and solvent molecules in the $S_1$ state and $S_1 \rightarrow S_0$ transition energies $\Delta E_{1\rightarrow 0}$ of the complexes (in kcal/mol).

| | Acetone | | $CH_2Cl_2$ | |
|---|---|---|---|---|
| Calculation level | $E_{int}$ | $\Delta E_{1\rightarrow 0}$ | $E_{int}$ | $\Delta E_{1\rightarrow 0}$ |
| ωB97X-D/6-31G(d,p) | −28.45 | 16.80 | −18.35 | 22.32 |
| ωB97X-D/6-311G(d,p) | −16.00 | 19.94 | −17.56 | 24.71 |
| PCM-ωB97X-D/6-31G(d,p) | −10.54 | 36.88 | −7.04 | 63.75 |
| PCM-ωB97X-D/6-311G(d,p) | −8.78 | 39.17 | −7.46 | 63.73 |

Table 5. Calculated interaction energies $E_{int}$ and $S_1 \rightarrow S_0$ transition energies $\Delta E_{1\rightarrow 0}$ of two aggregated enol HBT molecules in the $S_1$ state (in kcal/mol).

| Conformer | 1 | 2 | 3 | 4 | enol HBT | keto HBT |
|---|---|---|---|---|---|---|
| $E_{int}$ | −18.87 | −17.49 | −16.06 | −17.50 | | |
| $\Delta E_{1\rightarrow 0}$ | 69.52 | 72.77 | 76.95 | 70.12 | 77.14 | 64.78 |

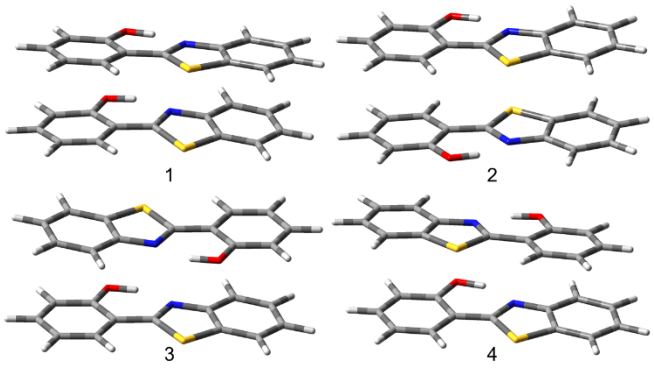


Figure 9. Optimized geometries of four conformers of aggregated HBT molecules at the ωB97X-D/6-31G(d,p) level.

Next, we calculated the interaction energies between the keto form of HBT and the solvent molecules. Only acetone and $CH_2Cl_2$ molecules were considered, because DMSO prevents ESIPT. In addition, we investigated the $S_1 \rightarrow S_0$ transition energies at the optimized geometries to determine the relaxation path. Table 4 summarizes the calculated results. Unlike the case for enol HBT, all the interaction energies are considerably negative, indicating that keto HBT strongly interacts with the solvent molecules. The $S_1 \rightarrow S_0$ transition energies of complexes formed between keto HBT and acetone are considerably smaller than those formed between keto HBT and $CH_2Cl_2$. For example, the values at the PCM-ωB97X-D/6-31G(d,p) level are 36.88 and 63.75 kcal/mol for acetone and $CH_2Cl_2$, respectively. These results suggest that internal conversion is preferable in acetone solution, whereas fluorescence is dominant in $CH_2Cl_2$ solution, which is qualitatively consistent with the experimental results.

This large difference between acetone and $CH_2Cl_2$ comes from the optimized geometries (Figure 8). Keto HBT in acetone twists to form an intermolecular hydrogen bond between the N-H bond of HBT and the acetone carbonyl group. By contrast, keto HBT in $CH_2Cl_2$ solution is planar, and an intermolecular hydrogen bond forms between the carbonyl group of HBT and the $CH_2Cl_2$ C-H bond. Namely, the two solvents play different roles: acetone functions as a hydrogen-bond acceptor, whereas $CH_2Cl_2$ functions as a hydrogen-bond donor. When the keto HBT and solvent act as hydrogen-bond donor and acceptor respectively, keto HBT is twisted. Therefore, C=C twisting in keto HBT is controlled by whether the solvent is a hydrogen-bond donor or acceptor. It is noted that additional $CH_2Cl_2$ molecule can form a hydrogen bond with keto HBT acting as a hydrogen-bond acceptor. However, the $S_1 \rightarrow S_0$ transition energy of complex between keto HBT and two $CH_2Cl_2$ molecules (Fig. S5) are almost unchanged (Table S3).

**HBT aggregation**

Table 5 shows the interaction energies and the $S_1 \rightarrow S_0$ transition energies of two stacked enol HBT molecules in the $S_1$ state, which are calculated at the PCM(DMSO)-ωB97X-D/6-31G(d,p) level. Here, we considered four π-π stacking conformers (Figure 9). For comparison, the $S_1 \rightarrow S_0$ transition energies of enol and keto HBT are listed in Table 5. Conformer 1, in which two HBT molecules are stacked in the same direction, is found to be the most stable configuration. Therefore, the most probable stacking structure for HBT aggregation in DMSO solution is conformer 1. The $S_1 \rightarrow S_0$ transition energy of conformer 1 is smaller than that for enol HBT but larger than that of keto HBT. This result is consistent with the experimental fluorescence spectrum. Therefore, it is demonstrated that the second-most intense peak found in DMSO and DMSO/$H_2O$ solutions is induced by enol-HBT aggregation.

## Conclusions

We carried out DFT and TDDFT calculations to elucidate the solvent dependency mechanism of the HBT fluorescence spectrum. We calculated the energy profiles for intramolecular proton transfer and C=C twisting in DMSO, acetone, and $CH_2Cl_2$ solutions by using PCM. However, no remarkable solvent dependencies were observed, because PCM cannot be used to model the intermolecular hydrogen bond between a solute and a solvent. Therefore, we explicitly treated the solvent molecules and investigated the intermolecular hydrogen bonds. The hydrogen-bond acceptability of the solvent was found to determine whether ESIPT proceeds. DMSO has a high hydrogen-bond acceptability and forms an intermolecular hydrogen bond with HBT that prevents ESIPT. The enol form of HBT thus relaxes to the $S_0$ state, emitting the fluorescence corresponding to enol HBT in DMSO solution. By contrast, ESIPT proceeds in $CH_2Cl_2$ and acetone, which do not have high hydrogen-bond acceptabilities. In addition, C=C twisting in keto HBT is controlled by whether the solvent molecule is a hydrogen-bond donor or acceptor. C=C twisting proceeds in acetone, which, acts as a hydrogen-bond acceptor, thereby decreasing the $S_1 \rightarrow S_0$ transition energy. Therefore, internal conversion is the dominant relaxation process in acetone. Planar keto HBT is stable in $CH_2Cl_2$, which acts as a hydrogen-bond donor and relaxes to the $S_0$ state with fluorescence. Furthermore, the second-most intense peak in DMSO and DMSO/$H_2O$ solutions was found to be induced by the stacking of enol HBT in the direction that decreases the $S_1 \rightarrow S_0$ transition energy. Note that as TDDFT cannot describe conical intersections, the $S_1 \rightarrow S_0$ transition energies could be further

decreased around the C=C twisted geometries. However, this decrease would not change the conclusions presented above.

HBT is a typical ESIPT molecule. HBT and HBT derivatives are used in various fields. In this study, the mechanisms of the solvent dependencies of HBT and the importance of solvent effects are elucidated. These findings are expected to be useful for molecular designs of novel HBT derivatives or other luminescent materials.

## Conflicts of interest

There are no conflicts to declare.

## Acknowledgements

This study was supported by JSPS KAKENHI Grant Numbers JP16KT0165, JP17K05757, JP18H04657, JP20H04813, JP20H05099, and JP20H05839. Some computations were performed at the Research Center for Computational Science, Okazaki, Japan.

## Notes and references

1 K. I. Sakai, T. Ishikawa and T. Akutagawa, *J. Mater. Chem. C*, 2013, **1**, 7866–7871.

2 S. Furukawa, H. Shono, T. Mutai and K. Araki, *ACS Appl. Mater. Interfaces*, 2014, **6**, 16065–16070.

3 H. Shono, T. Ohkawa, H. Tomoda, T. Mutai and K. Araki, *ACS Appl. Mater. Interfaces*, 2011, **3**, 654–657.

4 W. Sun, S. Li, R. Hu, Y. Qian, S. Wang and G. Yang, *J. Phys. Chem. A*, 2009, **113**, 5888–5895.

5 V. S. Padalkar and S. Seki, *Chem. Soc. Rev.*, 2016, **45**, 169–202.

6 S. Sahana, G. Mishra, S. Sivakumar and P. K. Bharadwaj, *Dalt. Trans.*, 2015, **44**, 20139–20146.

7 A. C. Sedgwick, L. Wu, H. H. Han, S. D. Bull, X. P. He, T. D. James, J. L. Sessler, B. Z. Tang, H. Tian and J. Yoon, *Chem. Soc. Rev.*, 2018, **47**, 8842–8880.

8 Q. Chen, C. Jia, Y. Zhang, W. Du, Y. Wang, Y. Huang, Q. Yang and Q. Zhang, *J. Mater. Chem. B*, 2017, **5**, 7736–7742.

9 S. M. Aly, A. Usman, M. Alzayer, G. A. Hamdi, E. Alarousu and O. F. Mohammed, *J. Phys. Chem. B*, 2015, **119**, 2596–2603.

10 T. Elsaesser and B. Schmetzer, *Chem. Phys. Lett.*, 1987, **140**, 293–299.

11 T. Elsaesser, B. Schmetzer, M. Lipp and R. J. Bäuerle, *Chem. Phys. Lett.*, 1988, **148**, 112–118.

12 W. E. Brewer, M. L. Martinez and P. T. Chou, *J. Phys. Chem.*, 1990, **94**, 1915–1918.

13 W. K. F. Laermer, T. Elsaesser, *Chem. Pys. Lett.*, 1988, **148**, 119–124.

14 S. Pijeau, D. Foster and E. G. Hohenstein, *J. Phys. Chem. A*, 2017, **121**, 4595–4605.

15 R. De Vivie-Riedle, V. De Waele, L. Kurtz and E. Riedle, *J. Phys. Chem. A*, 2003, **107**, 10591–10599.

16 P. Purkayastha and N. Chattopadhyay, *Phys. Chem. Chem. Phys.*, 2000, **2**, 203–210.

17 M. Barbatti, A. J. A. Aquino, H. Lischka, C. Schriever, S. Lochbrunner and E. Riedle, *Phys. Chem. Chem. Phys.*, 2009, **11**, 1406–1415.

18 H. Roohi, N. Mohtamedifar and F. Hejazi, *Chem. Phys.*, 2014, **444**, 66–76.

19 M. Iravani and R. Omidyan, *J. Phys. Chem. A*, 2018, **122**, 3182–3189.

20 R. Nakagaki, T. Kobayashi and S. Nagakura, *Bull. Chem. Soc. Jpn.*, 1978, 51, 1671–1675.

21 M. Itoh and Y. Fujiwara, *J. Am. Chem. Soc.*, 1985, **107**, 1561–1565.

22 D. McMorrow and M. Kasha, *J. Phys. Chem.*, 1984, **88**, 2235–2243.

23 P. K. Sjzngupta and M. Kasha, *Chem. Phys. Lett.*, 1979, **68**, 382–385.

24 J. S. Baskin, L. Bañares, S. Pedersen and A. H. Zewail, *J. Phys. Chem.*, 1996, **100**, 11920–11933.

25 C. H. Choi and M. Kertesz, *J. Phys. Chem. A*, 1997, **101**, 3823–3831.

26 J. Quenneville and T. J. Martínez, *J. Phys. Chem. A*, 2003, **107**, 829–837.

27 R. Send and D. Sundholm, *J. Phys. Chem. A*, 2007, **111**, 8766–8773.

28 C. Schnedermann, M. Liebel and P. Kukura, *J. Am. Chem. Soc.*, 2015, **137**, 2886–2891.

29 V. I. Prokhorenko, A. M. Nagy, R. J. Dwayne Miller and L. S. Brown, *Opt. InfoBase Conf. Pap.*, 2006, 1257–1262.

30 S. Miertuš, E. Scrocco and J. Tomasi, *Chem. Phys.*, 1981, **55**, 117–129.

31 B. Mennucci, *Wiley Interdiscip. Rev. Comput. Mol. Sci.*, 2012, **2**, 386–404.

32 F. Lipparini and B. Mennucci, *J. Chem. Phys.*, , DOI:10.1063/1.4947236.

33 J. Da Chai and M. Head-Gordon, *Phys. Chem. Chem. Phys.*, 2008, **10**, 6615–6620.

34 R. Peverati and D. G. Truhlar, *J. Phys. Chem. Lett.*, 2011, **2**, 2810–2817.

35 R. J. Bartlett and M. Musiał, *Rev. Mod. Phys.*, 2007, **79**, 291–352.

36 M. J. Frisch, G. W. Trucks, H. B. Schlegel, G. E. Scuseria, M. a. Robb, J. R. Cheeseman, G. Scalmani, V. Barone, G. a. Petersson, H. Nakatsuji, X. Li, M. Caricato, a. V. Marenich, J. Bloino, B. G. Janesko, R. Gomperts, B. Mennucci, H. P. Hratchian, J. V. Ortiz, a. F. Izmaylov, J. L. Sonnenberg, Williams, F. Ding, F. Lipparini, F. Egidi, J. Goings, B. Peng, A. Petrone, T. Henderson, D. Ranasinghe, V. G. Zakrzewski, J. Gao, N. Rega, G. Zheng, W. Liang, M. Hada, M. Ehara, K. Toyota, R. Fukuda, J. Hasegawa, M. Ishida, T. Nakajima, Y. Honda, O. Kitao, H. Nakai, T. Vreven, K. Throssell, J. a. Montgomery Jr., J. E. Peralta, F. Ogliaro, M. J. Bearpark, J. J. Heyd, E. N. Brothers, K. N. Kudin, V. N. Staroverov, T. a. Keith, R. Kobayashi, J. Normand, K. Raghavachari, a. P. Rendell, J. C. Burant, S. S. Iyengar, J. Tomasi, M. Cossi, J. M. Millam, M. Klene, C. Adamo, R. Cammi, J. W. Ochterski, R. L. Martin, K. Morokuma, O. Farkas, J. B. Foresman and D. J.

Fox, 2016, Gaussian 16, Revision C.01, Gaussian, Inc., Wallin.

37 T. Mutai, H. Sawatani, T. Shida, H. Shono and K. Araki, *J. Org. Chem.*, 2013, **78**, 2482–2489.

38 A. Abkowicz-Bieńko, M. Biczysko and Z. Latajka, *Comput. Chem.*, 2000, **24**, 303–309.

39 J. A. Gauthier, S. Ringe, C. F. Dickens, A. J. Garza, A. T. Bell, M. Head-Gordon, J. K. Nørskov and K. Chan, *ACS Catal.*, 2019, **9**, 920–931.

40 P. Bandyopadhyay and M. S. Gordon, *J. Chem. Phys.*, 2000, **113**, 1104–1109.